The FERMI@Elettra free-electron-laser source for coherent X-ray physics: photon properties, beam transport system, and applications

E Allaria[1], C Callegari[1], D Cocco[1], W M Fawley[1,2], M Kiskinova[1], C Masciovecchio[1] and F Parmigiani[1,3]

[1] Sincrotrone Trieste S.C.p.A., Trieste (Italy)
[2] Lawrence Berkeley National Laboratory, Berkeley, CA (USA)
[3] Dipartimento di Fisica, Università di Trieste (Italy)

E-mail: fulvio.parmigiani@elettra.trieste.it

Abstract. FERMI@Elettra is comprised of two free electron lasers (FELs) that will generate short pulses ($\tau \sim 25$ to 200 fs) of highly coherent radiation in the XUV and soft X-ray region. The use of external laser seeding together with a harmonic upshift scheme to obtain short wavelengths will give FERMI@Elettra the capability to produce high quality, longitudinal coherent photon pulses. This capability together with the possibilities of temporal synchronization to external lasers and control of the output photon polarization will open new experimental opportunities not possible with currently available FELs. Here we report on the predicted radiation coherence properties and important configuration details of the photon beam transport system. We discuss the several experimental stations that will be available during initial operations in 2011, and we give a scientific perspective on possible experiments that can exploit the critical parameters of this new light source.

PACS: 41.60.Cr, 42.72.-g

1. Introduction

The dynamics and temporal evolution of matter down to sub-femtosecond time scales and atomic space scales are at the base of all chemical, physical and biological processes [1]. Consequently, the past couple decades have seen an impressive quest for tools capable of temporally resolving ultrafast processes related to the dynamics of the electronic interaction with other electrons or phonons, photons, magnons and polarons [2]. The characteristic time scales span from as short as attoseconds in the case of electronic processes at the core levels in atoms, to a few femtoseconds for the electron dynamics at the valence band, and to as large as a few picoseconds, as in the case of processes that involve interactions with heavy particles such as phonons [2].

The drive towards shorter time scales has been accompanied by a push to probe the structure and chemistry of transient events at their natural nanometer and sub-nanometer length scales [3]. In this respect, coherent light sources have enabled imaging with diffraction-limited spatial resolution and can be a powerful tool to resolve the structure, chemistry, and energetics of single functional units. Thanks to a new generation of fully coherent laser sources with short pulses and high peak brightness, it has now become possible to obtain simultaneously both high temporal and spatial resolution [4]. However, conventional lasers emit radiation only in a limited wavelength range and their use is, in general, restricted to optical and spectroscopic techniques in the infrared, visible, and near-ultraviolet range, thus excluding all measurements that require photon energy higher than a few eV. The desire to extend this range to the XUV and harder energies dates back to the time of the first functioning lasers and includes many attempts to generate coherent X-ray pulses starting with ultrashort pulses from infrared (IR) lasers [5]. More recently, interest has turned to short wavelength, free electron lasers (FEL) [6] which can produce light pulses with peak brilliance up to ten orders of magnitude higher than the pulses generated in present third generation synchrotron light sources and with photon energies spanning from the vacuum ultraviolet to

the hard X-ray, *i.e.*, from about 10 eV (120 nm) to 10 keV (0.12 nm).
FEL sources can operate in several ways. To date, most existing and planned very short wavelength FELs (*e.g.,* FLASH, LCLS, SCSS, XFEL, SPARX) have employed the SASE (Self Amplification of Spontaneous Emission) [7] mode of operation. While it is possible to get extremely high brilliance, the temporal structure of a SASE output pulse is normally composed of a series of micro-pulses that individually have random phase and highly fluctuating peak intensity and time duration. For SASE devices, synchronism to external sources is normally limited by the temporal jitter of the accelerator. This jitter can be tens of femtoseconds or greater, especially for accelerators based upon non-superconducting cavities. As an alternative, short wavelength FEL sources based upon "seeding" techniques in which the FEL pulse is initiated by a coherent radiation pulse generated by a conventional laser can produce output pulses with a well-defined temporal shape and intensity stability [8,9] that permits relatively straight-forward synchronization with external pump or probe lasers. In principle, seeded FELs can obtain output radiation bandwidths close to the Fourier Transform Limit. In this paper, we describe a new light source currently under construction, FERMI@Elettra [10], comprised of two FELs that will use a combination of coherent seeding and harmonic upshifting [11,12] to provide coherent emission over a photon energy range of 12-300 eV (and up to 900 eV at the third harmonic). We note as an indication of the attractiveness of this approach, other groups such as the s-FLASH project at DESY [13] are also actively investigating short wavelength seeded FEL sources.

The remainder of this paper is organized as follows. Section 2 summarizes the basic physics principles of the FERMI FEL sources and gives a characteristic sample of the numerical simulation predictions for the expected output radiation coherence properties. Section 3 presents the FERMI photon beam transport and diagnostic systems. We conclude with Section 4, that overviews the principal instruments which will make it possible to reach the scientific goals enabled by FERMI's intense, highly coherent radiation pulses in the XUV and soft X-ray region. These include temporally synchronized pump-probe experiments and others involving third harmonic radiation with photon energies as high as 900 eV.

2. FERMI's Harmonic Cascade Approach to Short Wavelength Generation

2.1 Basic Physics Principle and Configuration
The two FERMI [10] free-electron lasers are based upon the principle of harmonic upshifting [11,12] of an initial, coherent radiation "seed" signal within a single pass, FEL amplifier configuration employing multiple undulators. FERMI's FEL-1 will cover the low energy photon spectral range (20-100 nm, *i.e.*, 12-60 eV) using a single stage harmonic upshift while FEL-2 uses two upshift stages to reach output wavelengths (fundamental) as short as 4 nm (*i.e.*, 300 eV). Each upshift stage begins with a relatively short magnetic undulator (the "modulator"), in which a coherent radiation input signal imprints a relatively strong, coherent energy modulation on the electron beam whose magnitude is much greater than the initial uncorrelated energy spread σ_E. For FERMI's FEL-1 and the first stage of FEL-2, the input signal is provided by a wavelength-tunable, high power, external UV laser (see Table 1). Following the modulator is a relatively weak chromatic dispersion section (R_{56} ~ 40 microns or less) that converts the energy modulation into a coherent density modulation with strong harmonic overtones. Finally, each upshift stage culminates with a "radiator" undulator whose normalized RMS magnetic strength a_w is tuned such that FEL resonance occurs at a radiation wavelength that is an integral harmonic h of the original input wavelength,

$$\lambda_R = \lambda_0/h = \lambda_w \cdot (1 + a_w^2) / 2\gamma^2 \quad (1)$$

where λ_w is the undulator period and γ is the electron relativistic Lorentz factor. In both the radiators of FEL-1 and the first stage of FEL-2 we plan to use *h* in the range 2 to 12. The second stage of FEL-2, whose initial input radiation signal is the output from the first stage

radiator, will likely be limited by σ_E to a maximum $h \leq 5$. FERMI will employ the "fresh bunch" approach [14] for FEL-2, thus requiring a delay chicane between the two stages. This choice together with the currently expected accelerator pulse timing jitter levels and e-beam pulse length will likely limit useful seed and output pulse durations to 200 fs or less.

The radiators of both FEL-1 and the second stage of FEL-2 are many exponential gain lengths long and are expected to lead to FEL power saturation, as in the classic high gain harmonic generation scheme described by Yu [12]. By contrast, the first stage radiator of FEL-2 is significantly shorter (~2 gain lengths or less) because the needed input power for the second stage modulator is much less than that corresponding to saturation. Consequently, there is a 2× or less increase of the microbunching from entrance to exit, and the resulting radiation is essentially coherent spontaneous emission of a prebunched electron beam.

2.2 Predicted Coherence Properties of the FERMI FEL-2 Harmonic Cascade

Much of the interest in harmonic cascade FELs over the past decade has stemmed from their promise of producing pulses with a much higher degree of temporal coherence than is normally possible from SASE FELs. While SASE output can have nearly full transverse coherence, the longitudinal coherence is generally limited to a length $l_c \sim (L_G/\lambda_w) * \lambda_R$, where the term in parentheses is of order 50-1000 for reasonably high gain devices. At 4-nm output wavelength, $l_c / c \leq 13$ fs. This limitation arises from the physics of the SASE process and not from imperfections of the electron beam (*e.g.*, energy chirp, current ripples) or the magnetic undulator. By contrast, a harmonic cascade FEL, presuming a perfect external laser seed and an electron beam without any macroscopic variations, can in principle produce a nearly transform-limited output pulse with coherence lengths exceeding 100-fs.

To illustrate the differences in the coherence properties between SASE and that possible with FERMI's FEL-2 operating as a seeded cascade, we have done a series of numerical simulations with the GINGER simulation code [15] using the seed and electron beam parameters listed in Table 1. The comparison has been done for an output wavelength of 4.2 nm (*i.e.,* near the K-edge of C). This is close to the shortest wavelength of operation for FERMI FEL-2 and thus will be fairly sensitive to non-ideal electron beam properties. There are 3 different simulation cases: the first involves a SASE configuration with an ideal, time-steady e-beam and a single undulator, the second employs a two stage harmonic cascade (208 nm → 21 nm → 4.2 nm) again using an ideal e-beam, and the third is identical to the second but uses macroparticles from a "start-to-end" (S2E) tracking code simulation of the FERMI electron beam, beginning at the injector and ending at the undulator entrance. The S2E simulation includes the effects of the longitudinal space-charge microbunching instability [16] which leads to temporally-localized fluctuations in beam energy and current; however, the noise level from which the instability grows was not initialized according to Poisson statistics and thus the fluctuation levels may be significantly over-estimated.

Figures 1a-c show the output power profile as a function of time for the three simulation cases. The SASE power (figure 1a) strongly fluctuates within the 115-fs wide simulation window around a mean level of ~ 2 GW with approximately 25 individual spikes. The seeded double cascade case with an ideal electron beam (figure 1b) has a very smooth output pulse with a FWHM of ~80 fs, slightly smaller than that of the input seed. The double cascade case with non-ideal, S2E electron beam (figure 1c) has a *P(t)* profile that is much less smooth, displaying oscillations at the ±25% level.

Near-field power spectra (figure 2a-c) show a similar range of differences: the SASE case is composed of multiple spikes ranging over ±0.0075 nm, the ideal e-beam cascade case has a single peak with a FWHM of 1.0×10^{-3} nm, and the non-ideal, S2E e-beam cascade case has a dominant spike of similar width but an equal amount of power is contain in a halo approximately three times larger. The reader should note that the exact details of radiation

output in the SASE and S2E cases are sensitive to the initial microbunching distributions and will thus vary from shot to shot.

To investigate the output radiation properties in more detail, we have calculated the Wigner transform W of the far field at the on-axis position (*i.e.*, θ=0). W effectively measures the local phase space density of the radiation and is defined as,

$$W(\omega,t) \equiv \int d\tau\, E^{*}(t-\tau/2)\times E(t+\tau/2)\, e^{+i\omega\tau} \qquad (2)$$

The integration of W over t gives the on-axis power spectrum (times a constant factor) while the integration over ω gives the instantaneous intensity (also times a constant factor). Figure 3a shows the false color image of the Wigner transform of the SASE output case. There is a chaotic structure in both time and frequency with many individual coherent "hot spots", each encompassing ~ 5×10^{-3} fs-nm in area. The disordered structure is indicative of random phase jumps between different intensity spikes. By contrast, the ideal beam, external laser seeded-cascade case (figure 3b) consists of one large and well-defined coherent region spanning ~ 100×10^{-3} fs-nm. The smoothness of the region is indicative of a smoothly varying phase. There is a noticeable linear chirp in wavelength with magnitude ~ -1.5×10^{-4} nm/fs. This chirp is a natural feature of FEL radiation from short pulses and tends to increase in magnitude as one approaches power saturation.

The S2E cascade case has a Wigner transform (figure 3c) that is far less ordered than the ideal beam case, albeit far smoother and more confined than the SASE case. Here the effective coherence time is reduced from the ~20-fs value of the ideal e-beam case to ~5-fs. The underlying cause for the apparent breakup from a single region in the ideal beam case to ~5 topologically distinct regions in the S2E case is a relatively rapid (but ordered) phase variation arising from the interplay of ~3-fs period energy oscillations on the electron beam (due to microbunching instability growth upstream in the accelerator) with the strong chromatic dispersion region in the first harmonic cascade stage. As mentioned above, we have limited confidence that the initial noise level (*i.e.*, in the injector region) for these energy oscillations was correctly modeled by the tracking code simulations, whose output produced the input particle distributions for the FEL simulations. If the initial noise level is a factor two too high and/or if the first stage chromatic dispersion section strength was to be reduced by a similar factor (*e.g.*, by using a stronger external laser), the output phase oscillation amplitude would decrease by at least two and the number of distinct regions could shrink to two or possibly even one. Consequently, while it will certainly be difficult to get output radiation pulses approaching the near-perfection shown in figure 3b, we believe there are a number of "tuning knobs" for FERMI's FEL-2 that will produce output better than the S2E case shown in figure 3c (and far superior to the SASE case of figure 3a).

The transverse coherence for each of the cases presented here is quite good. The fraction of the power that is contained in a "best-fit" TEM_{00} mode is above 90% and the effective emission point in *z* (*i.e.*, best fit waist location) is typically ~5m before the saturation point in the undulator. The transverse coherence of the seeded S2E case is noticeably worse (albeit of still relatively good quality) than those found for the ideal e-beam SASE and seeded harmonic cascade cases; this difference may be due to a refractive guiding effect caused by the local energy chirp on the electron beam. All together, we have reasonably good confidence that the transverse coherence of the FERMI FEL-2 will be adequate for nearly all proposed experiments at wavelengths $\lambda \geq 4$ nm and will not require spatial filtering.

2.3 Third Harmonic Emission

We currently believe that the FERMI linear RF accelerator in its present configuration will have output electron energies limited to 1.5-GeV. For the particular choice of undulator

wavelength in the final radiator (*i.e.*, 35 mm), output power and photon number levels for fundamental wavelengths below ~4 nm will drop precipitously because the strong increase in the exponential gain length will prevent saturation by the end of the second radiator. Consequently, in order to reach photon energies in the 300-1000 eV range corresponding to L-edges of magnetically active elements (*e.g.*, Fe, Co), we plan to utilize third harmonic emission from FEL-2. When the final radiator is operated with linear or elliptical polarization, coherent emission at third and other odd harmonics occurs naturally with power levels approaching 0.1-0.5% that of the fundamental.

For the case of pure circular (helical) polarization, for aligned electron beams, there is negligible harmonic emission directly along the undulator axis. Coherent emission off axis is strongly (but not fully) suppressed by destructive interference effects. In order to produce reasonable power levels of higher harmonic, circularly-polarized emission on axis, we are currently examining a number of options possible with the Apple-2 undulator topology of the FERMI radiators. Most easily, we can operate the undulators with a slight (few percent level) amount of elliptical polarization. Experiments at the BESSY synchrotron light source [17] have shown that this configuration leads to relatively high levels of circularly-polarized emission on axis, both at the fundamental and odd harmonics, with small contamination (<10%) by linearly-polarized emission. A second possibility is the so-called cross-polarized mode [18] where undulator segments alternate between horizontal and vertical linear polarization (with appropriate phase shifts in between -- such phase shifters exist and are needed by the FERMI radiators for other reasons). This can produce quite strong circularly-polarized radiation at both the fundamental and odd harmonics, with predicted purity levels above 90% [19]. Finally, the magnetic field topology of the radiator undulator itself can be modified to have a large third harmonic component [20]. Such a modification can strongly enhance the coupling between the electron motion and third harmonic emission in all polarization modes without significantly affecting the emission at the fundamental. In a different context, similar topology modifications have been used to suppress harmonic emission [21].

We note that one need not make any of these suggested changes for all the radiator undulator segments. In general, since the FEL power exponentiates with undulator length in the final radiator, just changing the last couple undulator segments should be adequate. Near-term experiments on the ELETTRA storage ring FEL and FERMI's FEL-1 will allow us to investigate and optimize various options for enhanced, circularly-polarized harmonic emission. In terms of predicted coherence properties, our simulation studies and some externally seeded FEL experiments [8] have shown that the coherence length of the harmonic emission is reduced from that of the fundamental. There are at least two possible effects that can lead to this: 1) seeding with non-flat-top shapes (*e.g.*, parabolic or Gaussian profiles) in a high gain situation often leads to a reduced pulse width for the overall power at higher harmonics 2) if there are small eikonal phase variations on the fundamental of amplitude $\pm\Phi$, these will be increased by a factor h at harmonic number h [22]. The variations, once they approach a level of $\sim\pi$, limit the coherence length to values below that of the full radiation pulse. Conversely, to make sure the longitudinal coherence length at a higher harmonic h does not drop much when compared to the fundamental requires at least a reasonably flat temporal power profile and eikonal phase variations of amplitude $\ll\pi/h$.

Similar phenomena can be expected for the transverse coherence properties. For both SASE and seeded configurations, one expects a drop-off with radius in both the harmonic microbunching fraction and the corresponding harmonic emission strength. Thus the effective waist size r_h of the harmonic emission will be less than that found for the fundamental. This reduction appears to have been seen in coherent optical transition radiation (COTR) measurements at the LEUTL SASE experiment at Argonne [23]. The sensitivity to phase variations also applies transversely and may decrease the overall coherent power fraction contained in the TEM_{00} mode. Since the natural e-beam transverse shape is close to a Gaussian, there may be no simple way to prevent the effective waist size from decreasing

between the fundamental and higher harmonics. On the other hand, since the Rayleigh range at harmonic h scales directly with the factor ($h\ r_h^2$), the reduction in waist size tends to equalize the Rayleigh ranges; this might help with downstream experimental design.

Figure 4 summarizes the predicted output levels from FERMI's FEL-1 and FEL-2 as a function of final wavelength. The chosen electron beam parameters are those of Table 1 but with the current reduced to 750 A, transverse normalized emittance increased to 1.0 mm-mrad, and the incoherent energy spread increased to 500 keV (to take into account the effects of the energy modulation by the input radiation seed). The solid and dashed lines correspond to the predicted radiation energy for an output pulse of 40-fs duration that has reached saturation according to the Xie empirical formula [24]. Predictions at wavelengths below 3 nm correspond to the third harmonic emission in linear polarization. While there is non-negligible emission at the fifth harmonic, it typically is less than 1 part in 10^4 of the fundamental.

3. Photon beam transport system

The photon transport system of the FERMI project is divided into two distinct parts, a first one common to all the beamlines, called PADReS (Photon Analysis Delivery and Reduction system), and a second one consisting of the individual beamlines.

PADReS will be installed between the undulators and the beamlines (see figure 5). It has the dual purpose of delivering the radiation emitted by the two FELs to each experimental station and of characterizing on-line the pulse-by-pulse radiation. With the analysis system one can determine the absolute intensity of each pulse (*i.e.*, photons/pulse), the relative spatial position and angular tilt of the photon beam, and the pulse-resolved spectral distribution. Moreover, it will be possible to control the absolute intensity delivered to the beamlines via a 6 m long gas attenuation chamber with a maximum attenuation factor of 10^4. The information will be collected pulse by pulse and made available for the user in real time and also stored for future data reduction. A system of plane mirrors will deflect the radiation of both FELs (only one operates at a given time) to each of the three presently approved beamlines: DIPROI, dedicated to diffraction and projection imaging, LDM, dedicated to the study of diluted system, and EIS, dedicated to Elastic Scattering.

PADReS is comprised of the following components: a shutter, a beam-defining aperture, a beam position monitor, an intensity monitor, and a differentially-pumped gas adsorption cell. After the gas adsorption cell, the system is symmetrically repeated, with a second differential pumping system, a second intensity monitor, a second beam position monitor and then the first mirror. Inside the safety hutch, a system of three mirrors, two for FEL-1 and one for FEL-2, deliver the radiation to the on-line photon energy spectrometer. This analyzes, shot by shot, the energy spectrum of the emitted radiation. Starting from this point the light can be deflected to the Timer part of the EIS beamline (at whose beginning a system to measure the coherence of the beam will be installed) or go straight to the LDM, DIPROI or Timex-EIS beamlines that share a number of components.

The Timer-EIS beamline will work without a monochromator, while its use is optional on the Timex-EIS, LDM and DIPROI beamlines. The latter can work without a monochromator because the emitted photon number at the fundamental wavelength exceeds by a factor of 100 or more that emitted at higher harmonics. Consequently, the spectral purity of the non-monochromatized radiation beam is good enough to perform most experiments without having to suffer the additional efficiency loss associated with a monochromator. However, there will be a problem in selecting individual higher harmonics for experiments that need higher photon energy. These include pump and probe experiments in which one pumps the system at the fundamental wavelength and then probes it with the 3rd harmonic. Our solution, although useful for only a limited number of wavelengths, is to use multilayer reflective surfaces. The multilayers are optimized to work at one particular wavelength while

simultaneously having the smallest possible efficiency at a wavelength 3 times larger. In this way, for instance, a Co/C multilayer has 60 times more efficiency at 6.66 nm than at 20 nm wavelength. After 2 mirrors a reduction of more than 3000 is obtained; after 4 mirrors a factor of 10^7 can be reached. Depending on the degree of spectral purity needed, one can use wavefront and time-preserving multilayer mirrors instead of a complicated and costly grating-based monochromator to select the proper harmonic.

The roll in-roll out monochromator for the Timex-EIS, LDM and DIPROI beamlines is based upon a constant included angle scheme. The details of the calculations made for its design are described elsewhere [25]. Here we wish just to mention the reasons for such a choice and a few details. The request from users was to have a relatively low resolution, to be able to select one harmonic and to suppress the background associated with undulator spontaneous emission and the beam dump bending magnet radiation. Meanwhile, one should try to maximize the fluence, reducing or completely avoiding (if possible) time elongation of the output pulses. The solution adopted is a fixed angle monochromator (174°) involving three interchangeable gratings that will cover wavelengths from 80 down to 1 nm with a single movement (a rotation). Longer wavelengths will be used in zero order (non-dispersive).

A removable collimating mirror before the gratings system and a focusing mirror just after the gratings will guarantee a stigmatic focus at a fixed exit slit. If these two mirrors are removed, the radiation beam travels unchanged to a subsequent delay line. The delay line will split the beam into two parts. One part can be delayed relative to the other by up to 30 ps by using grazing incidence optics. A larger delay requires the introduction of a multilayer. With this system, one can also perform two-color experiments, with or without delay. The delay can be controlled with a minimum step of 0.3 fs. To guarantee the stability of the direction of the beam, a closed loop system (using a quadrant photodiode) is coupled to piezo correctors that act directly upon the mirrors that generate the time delay.

After the delay line, the beam can be directed to LDM, DIPROI or Timex-EIS beamlines. The Timex-EIS branch consists of a plane deflecting optics and a fixed focus elliptical mirror. Vice versa, the LDM and DIPROI will consist of two custom made active mirrors mounted in a Kirkpatrick-Baez configuration. The use of active optics providing shape control is necessary to compensate for the movement of the exit slit as well as the difference in distance between the source position of FEL-1 and FEL-2 (15 or more meters). Another reason for these optics is the need for an ability to change the spot dimension in the experimental chamber as desired. With these mirrors we will be able to go from a perfect unfocussed beam (several mm across) down to a micron size spot. Moreover, these mirrors are also wave front preserving optics. This is made possible by several actuators mounted in the back of the mirror surface. They not only preserve the wavefront and coherence of the incoming beam (by correcting mid frequency shape error of the mirror) but also compensate for deformation of the wave front due to the previous optics.

With such mirrors, we expect to have a spot size in the experimental chamber of the order of 2×3 μm^2, together with a very high fluence (i.e., power per unit area). Table 2 gives a fluence estimate for the DIPROI beamline, taking into account the geometrical acceptance, the mirror reflectivity, and, of course, the spot dimension. It is clear that very high fluences, above 10^{17} W/cm^2, are expected at the longest wavelengths, but, even at shorter wavelengths (*e.g.*, 5 nm) the fluence is higher than 10^{16} W/cm^2.

4. Experimental stations

The results of the simulations presented above clearly show the superior performance of a seeded FEL in terms of pulse temporal structure, coherence, and photon polarization. In order to reach the full potential of FERMI@Elettra, we prepare for time-resolved experiments based on resonant coherent diffraction imaging, elastic and inelastic scattering, photon and electron spectroscopy and transient grating spectroscopy, which will monitor transient states and non-linear material responses at mesoscopic and nano-

scales, exploiting selection rules as well. The planned and under construction experimental stations, briefly described below, will give access to dynamic phenomena, such as excitation lifetimes, phase separation and nucleation, ultrafast magnetization, complex rearrangements of constituents in cells, multi-photon single and multiple ionization, *etc*.

4.1 Coherent diffraction imaging

The extraordinary opportunity for single-shot coherent diffraction (lens-less) imaging (CDI) [26], which has become an excellent probe for the transient sample structure evolving after an excitation pulse from a pump laser [27] or using different delay schemes [28], will be fully exploited at FERMI. The photon-energy tunability of a FEL adds chemical imaging via resonant coherent diffraction at the atomic absorption edges and, when combined with the variable circular or linear polarization available from FERMI, extends the information to spin and orbital momentum. FERMI's DIPROI beamline and end-station is designed to meet the requirements for performing numerous types of static and dynamic coherent imaging. It includes split-delay correlation system and focusing optics for imaging of single small objects that also adds the option for complementary projection imaging. The possible measurement modes are:

- Single-shot CDI for probing specimen structure with diffraction-limited resolution.
- Resonant CDI for 'chemical' imaging exploring 'dichroic' mechanisms as well.
- Single-shot dynamic CDI using back reflective mirror for probing non-repetitive phenomena (e.g. radiation-induced damage) on fs scales;
- Time-resolved CDI for probing transient nanoscale dynamics on fs to ns timescales using split FEL pulses with adjustable delay or short-pulse optical laser pump.

Stroboscopic imaging with fs time resolution can be used to explore ultrafast dynamics at nanometer length scales, such as fracture, phase fluctuations, motions in soft matter, changes in various forms of magnetic or electronic segregations, copolymer assemblies, *etc*. By splitting the pulse and simultaneously hitting the object from two directions, it is possible to explore stereo 3D imaging as well.

4.2 Elastic and inelastic scattering

The Elastic and Inelastic Scattering (EIS) experimental end-station will be dedicated to two different research projects: 1) TIME-Resolved spectroscopy of mesoscopic dynamics in condensed matter (TIMER); 2) ultrafast TIme-resolved studies of Matter under EXtreme and metastable conditions (TIMEX). For TIMER, the photon energy and brilliance of the FEL radiation will be used for transient grating (TG) formation in the sample with a nanometer scale spatial period [29]. This will be achieved by using two identical pulses impinging at the same time on the sample to create a standing wave that imposes a transient density modulation in the sample [30]. A third, delayed pulse at the third harmonic is then scattered by the TG. The scattering amplitude is related to the collective dynamics present in the system and can serve as a time-dependent monitor. The aim of TIMER is to experimentally access the mesoscopic range of dynamics that at present cannot be investigated by any alternative experimental technique. This ability would be extremely interesting because it could solve several open scientific problems regarding the physics of systems without translational invariance [31]. We stress the fact that the possibility to create and probe transient gratings with spatial periods in the nanometer range will also be extremely useful for the study of surfaces and interfaces, with potential applications in the study of thin films and nanostructured materials [32].

TIMEX will exploit the unique intensity, energy domain and time structure of the FEL radiation to probe metastable and/or excited matter under extreme conditions. In particular, the energy and intensity of the FERMI FEL radiation beam is suitable for an efficient, ultrafast heating of most bulk-like dense samples. The main idea is to use the FEL beam within a pump-probe scheme for time-resolved studies of the optical and soft X-ray properties of matter providing direct information regarding surfaces and bulk under extreme conditions.

Such experiments in the 0.1-10 ps range are relevant to a variety of physical and chemical phenomena including high-pressure and high-temperature phase transitions, applied material studies, understanding of chemical reaction and catalysis paths, planetary interiors, inertial confinement fusion, various forms of plasma production [33] in which energy is rapidly deposited into a solid, and non-equilibrium and metastable states of matter [34].

4.3 Low density matter

The high brilliance of FELs is an ideal match to experiments involving low-density matter (LDM). The LDM beamline has been designed for experiments with supersonic (atomic, molecular, and cluster) beams. Supersonic beams provide a relatively intense ensemble of non-interacting atoms and molecules, usually at a low and well characterized temperature [35]. Experiments on atoms and molecules will explore non-linear multiple-ionization processes, whose interpretation may calls for the development of novel theoretical approaches. For molecules, in addition, energy redistribution processes subsequent to excitation, fragmentation in particular, can be studied, from any well-defined initial state that can be prepared with the pump laser. The close-to-ideal pulse structure (time as well as energy profile) will greatly expand the range of experiments and facilitate their interpretation as compared to a SASE source such as FLASH [36]. Clusters will be studied both as providing complementary information to supported samples such as those investigated in TIMEX and DIPROI experiments (note in particular the fact that TIMEX experiments imply isochoric heating, as opposed to isobaric in bare clusters) and for their intrinsic properties.

Of particular interest is that many materials non-magnetic in bulk form become magnetic in cluster form but the mechanisms are largely unknown [37]. Also, ultrafast changes of magnetization can be caused by slight changes of lattice parameters [38], usually induced with a femtosecond time scale laser pulse. The LDM beamline is ideally matched to perform this kind of experiment, especially by its ability to take advantage of the full control of the FEL pulse polarization. The LDM beamline has a further unique feature, namely the ability to produce beams of ultracold superfluid He nanodroplets (T=0.4K). These will be used both to study superfluidity at the nanoscale, and as a versatile substrate to assemble and cool heterogeneous molecular complexes that can then be studied via both one-color and pump-probe experiments (see, *e.g.,* [39] for a review of experiments with conventional lasers).

5. Conclusions

In this paper we have discussed various aspects of the FERMI@Elettra FEL design including its expected output coherence properties, the radiation beam transport system, and some possible experiments. Based upon the results of the numerical simulations we introduced here, the external seeded, harmonic upshift approach has clear advantages over a simple SASE design, with regards to longitudinal coherence. The photon transport system was designed to take maximum advantage of the source characteristics, preserving polarization, wave front, coherence and with the aim to maximize the fluence in the whole expected photon energy range. This was accomplished without precluding a possible upgrade to shorter wavelength.

FERMI will begin user operation in 2011 and, given its expected high transverse and longitudinal coherence together with variable polarization, should open the possibility of performing unique experiments at photon energies up to 900 eV. These will allow exploration of the structure and transient states of condensed, soft, and low density matter using a great variety of diffraction, scattering and spectroscopy techniques, and all temporal correlation modes.

Acknowledgments

We are pleased to acknowledge many useful discussions with our colleagues at Sincrotrone Trieste and elsewhere working on the FERMI project including W. Barletta, H. Chapman, P. Craievich, M. Cornacchia, M. Danailov, A. Di Cicco, B. Diviacco, S. DiMitri, G. DeNinno, A. Filipponi, J. Hajdu, S. Milton, T. Moeller, A. Nelson, M. Pelizzo, G. Penco, G. Penn, L.

Poletto, K. Prince, F. Stienkemeier, S. Stranges, C. Svetina, S. Tazzari, M. Zangrando and A. Zholents. C. Masciovecchio acknowledges the European Research Council for partially supporting the TIMER project through the Contract ERC No. 202804. Part of the work of W. Fawley was supported by the Office of Science, U. S. Department of Energy, under Contract No. DE-AC02-05CH11231 to LBNL.

References

[1] Zewail A H 2000 *J Phys. Chem A* **104** 5660
[2] Chergui M and Zewail A H 2009 *Chem. Phys. Chem.* **10** 28
[3] Cavalleri A *et al.* 2002 *Europhys. Lett.* **57** 281
Torre R, Bartolini P and Righini R 2004 *Nature* **428** 296
[4] Kapteyn H, Cohen O, Christov I and Murnane M 2004 *Science* **317** 775
Spence J 2007 *Nature* **449** 553
Kuroda D G, Singh C P Peng Z and Kleiman V D 2009 *Science* **326** 263
Buckup T, Hauer J and Motzkus M 2009 *New J. Phys.* **11** 105049
[5] Dunn J, Osterheld A L, Shepherd R, White W E, Shlyaptsev V N and Stewart R E 1998 *Phys. Rev. Lett*. **80** 2825
McPherson A, Gibson G, Jara H, Johann U, Luk T S, McIntyre I A, Boyer K and Rhodes C K 1987 *J. Opt. Soc. Am. B* **4** 595;
Ferray M, L'Huillier A, Li X F, Lompre L A, Mainfray G and Manus C 1988 *J. Phys. B: At. Mol. Opt. Phys.* **21** L31
[6] Madey J 1971 *J. Appl. Phys*. **42** 1906;
Deacon D A G, Elias L R, Madey J M J, Ramian G J, Schwettman H A and Smith T I 1977 *Phys. Rev. Lett*. **38**, 892
[7] Kondratenko A M and E. L. Saldin E L 1980 *Part. Accel.* **10** 207;
Bonifacio R, Pellegrini C, and Narducci L 1984 *Optics Comm*. **50** 373;
Kim K-J 1986 *Phys. Rev. Lett.* **57** 1871
[8] Yu L H *et al*. 2000 *Science* **289** 932
Yu L H *et al*. 2003 *Phys*. *Rev*. *Lett*. **91** 074801
[9] Doyuran A *et al*. 2004 *Phys. Rev. ST Accel. Beams* **7** 050701
Lambert G *et al*. 2008 *Nature Phys*. **4**, 296
[10] Bocchetta C J *et al*. 2007 *FERMI@Elettra Conceptual Design Report* **ST/F-TN-07/12** (Sincrotrone Trieste)
[11] Boscolo I and Stagno V 1980 *Nuovo Cimento B* **58** 267
Bonifacio R, de Salvo Souza L, Pierini P, Scharlemann E T 1990 *Nucl. Inst. Meth. A* **296**, 787
[12] Yu L H 1991 *Phys. Rev. A* **44** 5178
[13] Miltchev V *et al.,* 2009 *Proc*. *2009 FEL Conf*. **WEPC05**
[14] Ben-Zvi I, Yang, K M, and Yu L H 1992 *Nucl. Inst. Meth. A*, **318** 726
[15] Fawley W M 2004 LBNL Tech. Rpt. **LBNL-49625-Rev. 1** (also SLAC Rpt. **LCLS-TN-04-3**)
Fawley W M 2006 *Proc. 2006 Int. FEL Conf.* **MOPPH073**
[16] Saldin E L, Schneidmiller E A and Yurkov M V 2002 *Nucl. Instr. Meth. A* **483** 516
Huang Z and Kim K J 2002 *Phys. Rev. ST-AB* **5** 074401
Di Mitri S *et al*. 2009 *Nucl. Inst. Meth. A* **608** 19
[17] Khan S, Holldack K, Kachel T, Mitzner R and Quast T 2006 *Phys. Rev. Lett*. **97** 074801
[18] Kim K J 1984 *Nucl. Instrum. Meth.* **219** 425
Kim K J 2000 *Nucl. Instrum. Meth. A* **445** 329
[19] Ding Y and Huang Z 2008 *Phys. Rev. ST Accel. Beams* **11** 030702
Geng H, Ding Y and Huang Z 2009 *Proc.* 2009 *Part. Accel. Conf.* **WE5RFP042**
[20] Biedron S. *et al*. 2002 *Proc. SPIE* **4632** 50
Gottshalk S C 2004 *Proc. SPIE* **5534** 75
[21] Tanaka T and Kitmura H 1995 *Nucl. Instr. Meth. A* **364** 368
[22] Saldin E.L., Schneidmiller E A and Yurkov M V 2002 *Opt. Comm*. **202** 169
Fawley W M, Barletta, W A, Corlett J N. and Zholents A 2003 *Proc. 2003 Part. Accel Conf.*, **MPPB048**
[23] Lumpkin A H *et al*. 2003 *Nucl. Inst. Meth. A* **507** 200
[24] Xie M 2000 *Nucl. Inst. Meth. A* **445** 59
[25] Svetina, C, Zangrando M, Bianco A, and Cocco D 2009 *Proc. SPIE* **7448** 74480O
[26] Kirz J 2006 *Nature Physics* **2** 799
Gaffney K J and Chapman H N 2007 *Science* **316** 1444

[27] Abbey B *et al*. 2008 *Nature Physics* **4** 394
[28] Barty A *et al*. 2008 *Nature Photonics* **2** 415
Chapman H N 2007 *Nature* **448** 676
Grübel G *et al*. 2007 *Nucl. Instr. Meth. B* **262** 357
[29] Bencivenga F and Masciovecchio C 2009 *Nucl. Inst. and Meth. A* **606** 785
[30] Eichler H J, Gunter P and Pohl D W, 1986 *Laser-Induced Dynamic Gratings* (Berlin: Springer-Verlag)
[31] Balucani U and Zoppi M, 1994 *Dynamics of the Liquid State* (Oxford: Oxford Science Publications)
[32] Tobey R I, Siemens M E, Murnane M M, Kapteyn H C, Torchinsky D H and Nelson K A 2006 *Appl. Phys. Lett.* **89** 091108
[33] Lee R W *et al.* 2003 *J. Opt. Soc. Am. B* **20** 770
Lindenberg A M *et al*. 2005 *Science* **308** 392
[34] Mishima O and Stanley H E 1998 *Nature* **396** 329
[35] G Scoles G (ed.) 1988 (v.1)/1992 (v.2) *Atomic and Molecular Beam Methods* (Oxford University Press)
[36] W. Ackermann *et. al.,* 2007 *Nature Photonics* **1**, 336 - 342 ;
C. Bostedt *et al.* 2009 *Nucl. Inst. Meth. A* **601** 108
[37] Makarova T L 2010 "Nanomagnetism in Otherwise Nonmagnetic Materials", to appear in *Handbook of Nanophysics*, (K D Sattler, Ed.; Taylor&Francis Publisher --CRC Press)
[38] Wall S, Prabhakaran D, Boothroyd A T and Cavalleri A 2009 *Phys. Rev. Lett.* **107** 097402
[39] Stienkemeier F and Lehmann K K 2006 *J. Phys. B: At. Mol. Opt. Phys.* **39** R127

Table Captions

Table. 1 -- Nominal parameter values for the FERMI seed laser and electron beam.

Table. 2 -- Nominal values for the photon fluences expected at the DIPROI beamline. As no monochromator is present in this beamline, four multilayers are used to suppress the fundamental in order to deliver the 3rd harmonic to the experimental chamber.

Figure Captions

Figure 1 - Near-field instantaneous power as a function of time from FERMI FEL-2 as predicted by the GINGER simulation code at 4.2-nm wavelength from and electron beam with standard FERMI parameters. *Case (a):* Output from a SASE configuration over a time window of 115 fs with periodic boundary conditions. *Case (b*): An ideal (6D Gaussian) electron beam seeded by an external laser with 210-nm wavelength, 40-fs (RMS) Gaussian profile pulse. *Case (c):* Same as (b) except the input electron beam distribution came directly from "start-to-end" tracking code results.

Figure 2 - Predicted, near-field radiation power spectra for the three cases of Figure 1. The power levels depend upon the effective bin width *and* the temporal output window of the individual simulations and thus quantitatively cannot be compared directly.

Figure 3 - False color representations of the Wigner transform $W(\lambda,t)$ of the predicted, on-axis ($\theta=0$), far-field radiation output for the three cases of Figs. 1&2 (ideal e-beam + SASE, ideal e-beam + external seed, start-to-end e-beam + external seed). The numbers to the right of the plot refer to the false color scale bar (arbitrary units),

Figure 4 – Predicted output from FEL-1 and FEL-2 of FERMI as a function of output wavelength. The lines correspond to a 40-fs pulse reaching saturation according to the Xie empirical formulation [19] with the dashed lines (20-100 nm) corresponding to FEL-1 and the solid lines to FEL-2 (4-24 nm). Going from left to right, each set of three lines corresponds to electron beam energies of 0.9, 1.2, and 1.5 GeV. The isolated markers are results from detailed start-to-end (S2E) numerical simulation studies.

Figure 5 - Layout of the photon beam transport system of FERMI. From left to right there are the isolation vacuum valves, the beam-defining apertures, the beam position monitors, the radiation intensity monitors, the gas absorption cell, the three plane mirrors inside the safety hutch, the photon energy spectrometer, the EIS-Timer switching mirror, the removable monochromator, the delay line and the other currently approved beamlines with their switching and focusing systems.

Table 1: Nominal parameter values for the FERMI seed laser and electron beam

Parameter	**Value**	**Units**
Input Laser Wavelength	190 – 280	nm
Input Laser Pulse Length	40 – 70 (rms)	fs
Input Laser Peak Power	100	MW
Electron beam energy	0.9 – 1.5	GeV
Peak Current	750	A
Uncorrelated Energy Spread	150	keV
Norm. Transverse Emittance	0.8 – 1.0 (slice)	mm – mrad
Useful Bunch Length	600	fs

Table 2 . Nominal values for the fluence at the DIPROI beamline.

λ (nm)	FEL	Harmonic	Flux @ source (ph/pulse)	Flux @ sample (ph/pulse)	Fluence (W/cm^2)
1	2	3rd	$1.5x10^8$	$1.9x10^6$	$2.6x10^{11}$
1.4	2	3rd	$9.3x10^9$	$2.0x10^8$	$1.1x10^{13}$
1.67	2	3rd	$9.3x10^9$	$2.4x10^8$	$1.0x10^{13}$
3	2	1st	$3.5x10^{11}$	$4.7x10^{10}$	$2.1x10^{15}$
3.3	2	3rd	$5x10^{10}$	$1.9x10^9$	$7.8x10^{13}$
4	1	3rd	$1x10^9$	$4.3x10^7$	$3.4x10^{11}$
4.2	2	1st	$1.8x10^{12}$	$3.4x10^{11}$	$5.6\ x10^{15}$
5	2	1st	$3.3x10^{12}$	$8x10^{11}$	$1.1x10^{16}$
6.7	1	3rd	$1x10^{11}$	$1.6x10^{10}$	$7.6x10^{13}$
10	2	1st	$1x10^{13}$	$6.6x10^{12}$	$9.0x10^{16}$
20	2	1st	$5x10^{13}$	$3.3x10^{13}$	$2.3x10^{17}$
20	1	1st	$1x10^{13}$	$4.9x10^{12}$	$7.9x10^{15}$
40	1	1st	$4x10^{13}$	$2.0x10^{13}$	$1.6x10^{16}$
80	1	1st	$2x10^{14}$	$9.8x10^{13}$	$3.9x10^{16}$

Figure 1a

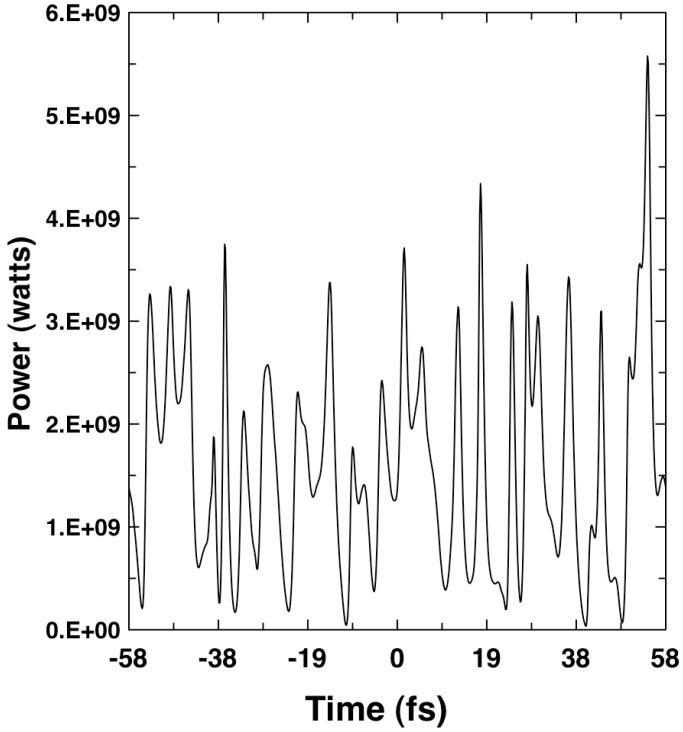
6.E+09
5.E+09
4.E+09
3.E+09
2.E+09
1.E+09
0.E+00
Power (watts)
-58
-38
-19
0
19
38
58
Time (fs)

Figure 1b

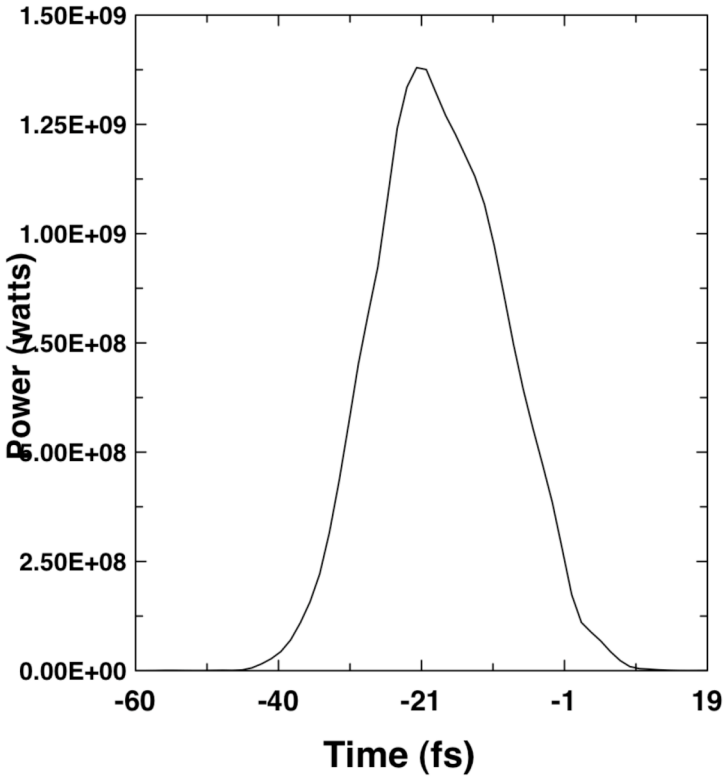
1.50E+09
1.25E+09
1.00E+09
5.00E+08
2.50E+08
0.00E+00
Power (watts)
-60
-40
-21
-1
19
Time (fs)

Figure 1c

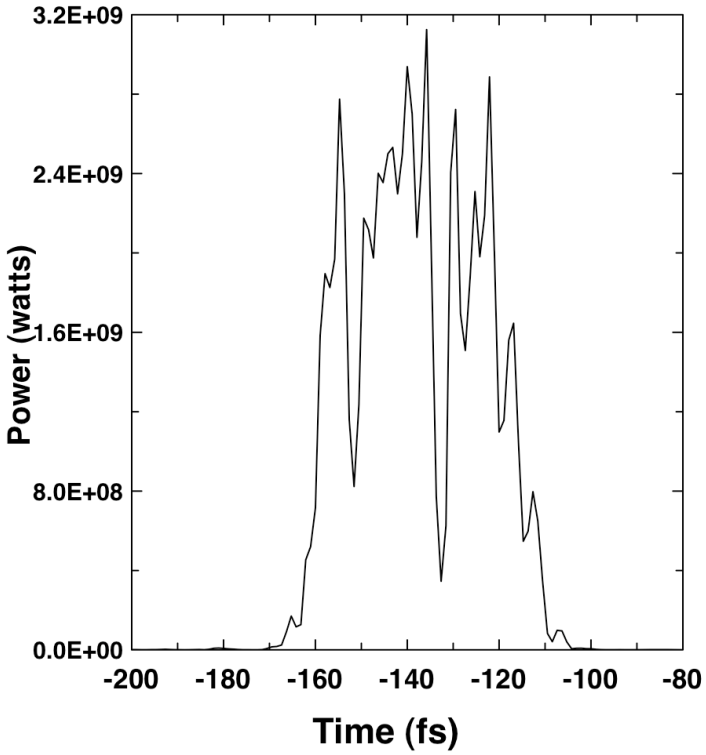
3.2E+09
2.4E+09
1.6E+09
8.0E+08
0.0E+00
Power (watts)
-200
-180
-160
-140
-120
-100
-80
Time (fs)

Figure 2a

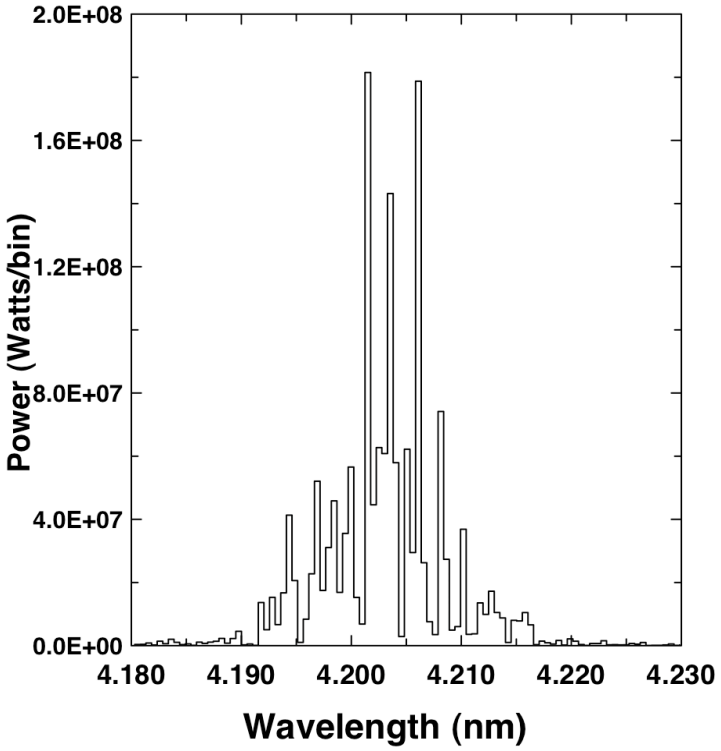
2.0E+08
1.6E+08
1.2E+08
8.0E+07
4.0E+07
0.0E+00
Power (Watts/bin)
4.180
4.190
4.200
4.210
4.220
4.230
Wavelength (nm)

Figure 2b

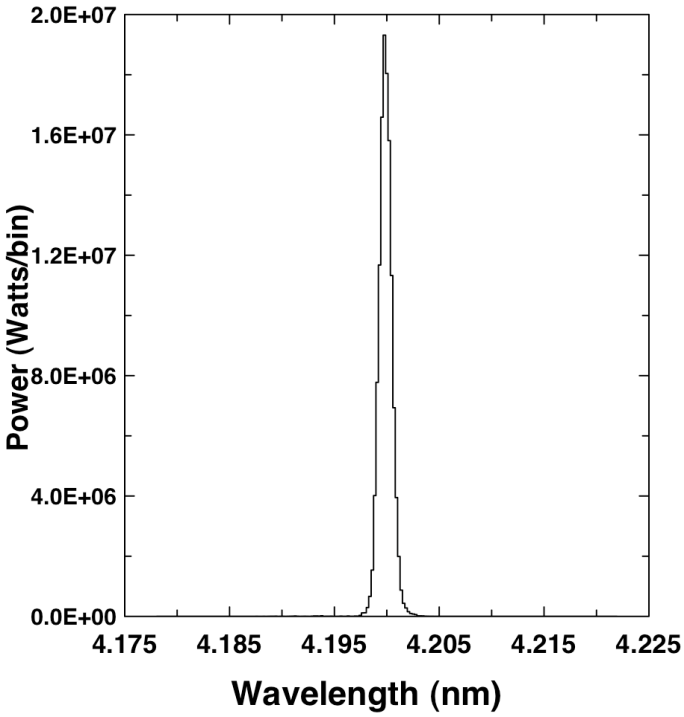
2.0E+07
1.6E+07
1.2E+07
8.0E+06
4.0E+06
0.0E+00
Power (Watts/bin)
4.175
4.185
4.195
4.205
4.215
4.225
Wavelength (nm)

Figure 2c

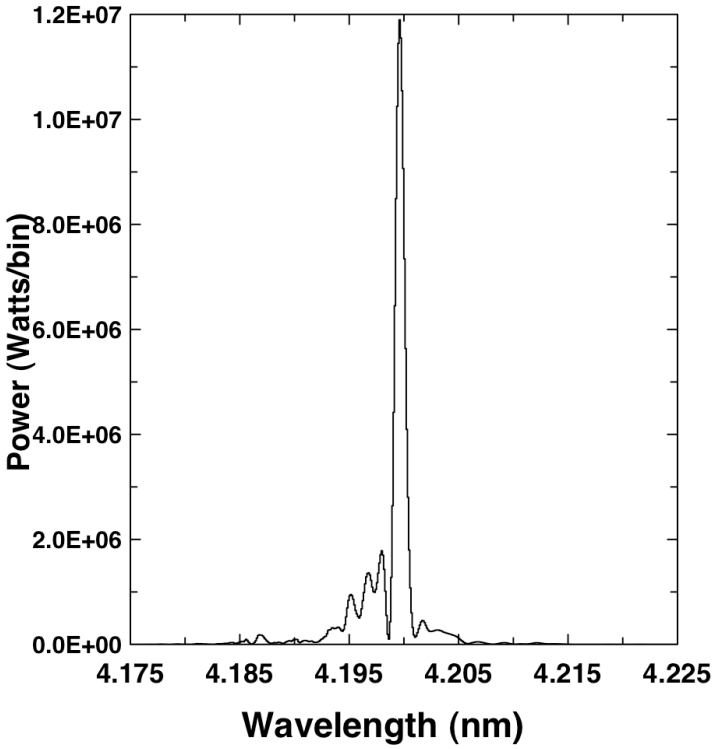
1.2E+07
1.0E+07
8.0E+06
6.0E+06
4.0E+06
2.0E+06
0.0E+00
Power (Watts/bin)
4.175
4.185
4.195
4.205
4.215
4.225
Wavelength (nm)

Figure 3a

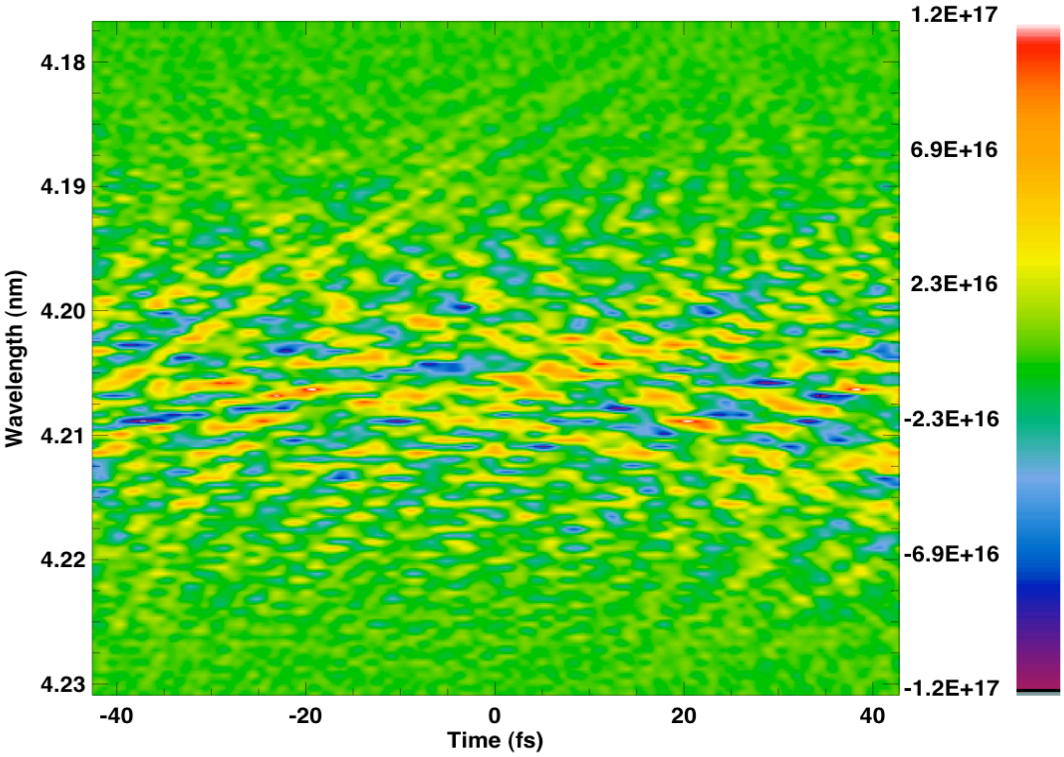
Wavelength (nm)
4.18
4.19
4.20
4.21
4.22
4.23
-40
-20
0
20
40
Time (fs)
1.2E+17
6.9E+16
2.3E+16
-2.3E+16
-6.9E+16
-1.2E+17

Figure 3b

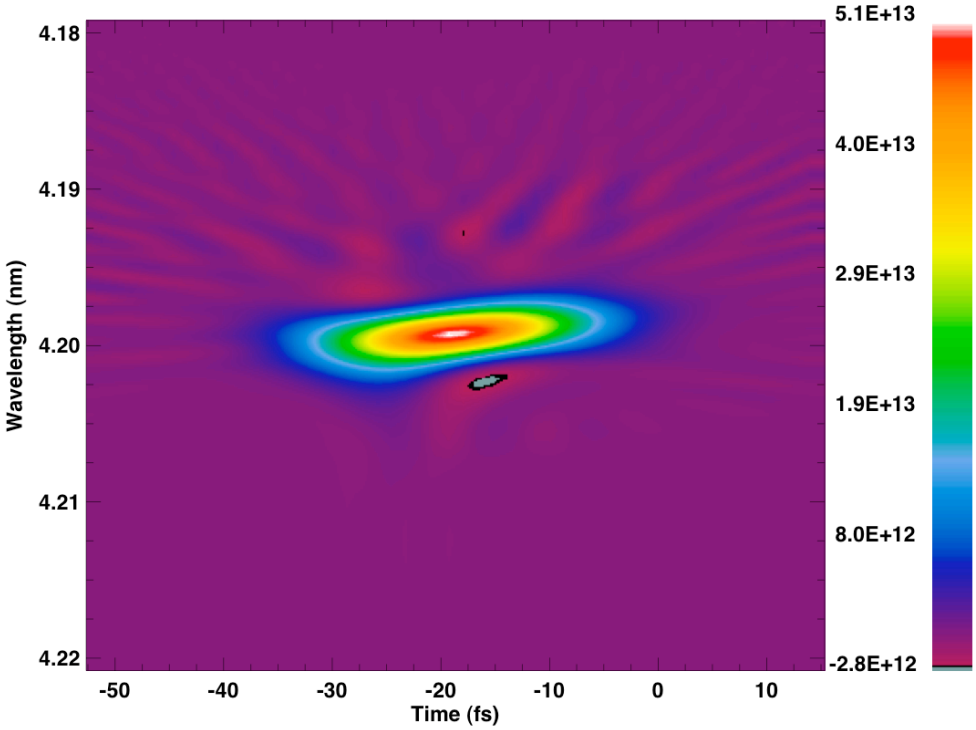
4.18
4.19
4.20
4.21
4.22
Wavelength (nm)
-50
-40
-30
-20
-10
0
10
Time (fs)
5.1E+13
4.0E+13
2.9E+13
1.9E+13
8.0E+12
-2.8E+12

Figure 3c

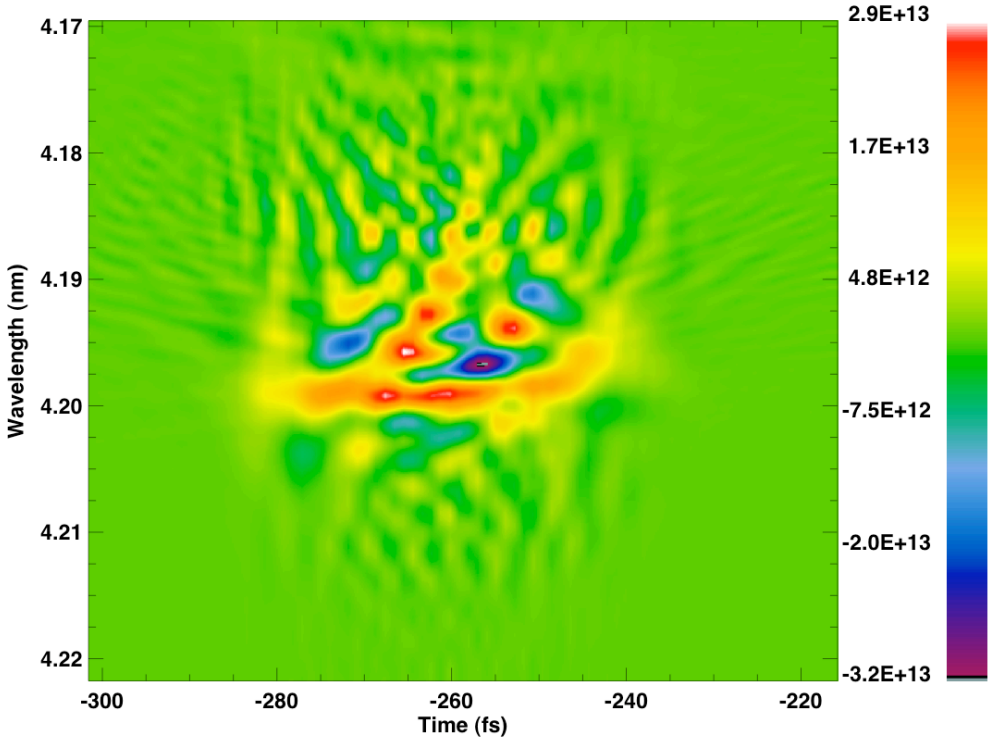
4.17
4.18
4.19
4.20
4.21
4.22
Wavelength (nm)
-300
-280
-260
-240
-220
Time (fs)
2.9E+13
1.7E+13
4.8E+12
-7.5E+12
-2.0E+13
-3.2E+13

Figure 4

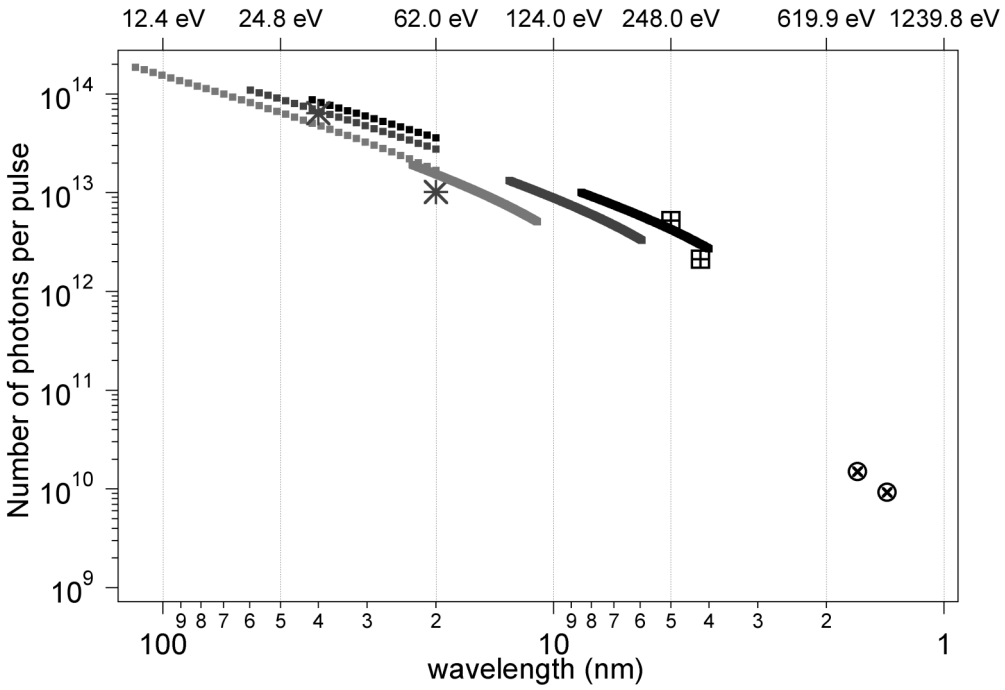
12.4 eV
24.8 eV
62.0 eV
124.0 eV
248.0 eV
619.9 eV
1239.8 eV
Number of photons per pulse
10^{14}
10^{13}
10^{12}
10^{11}
10^{10}
10^{9}
9 8 7 6 5 4 3 2
100
9 8 7 6 5 4 3 2
10
1
wavelength (nm)

Figure 5

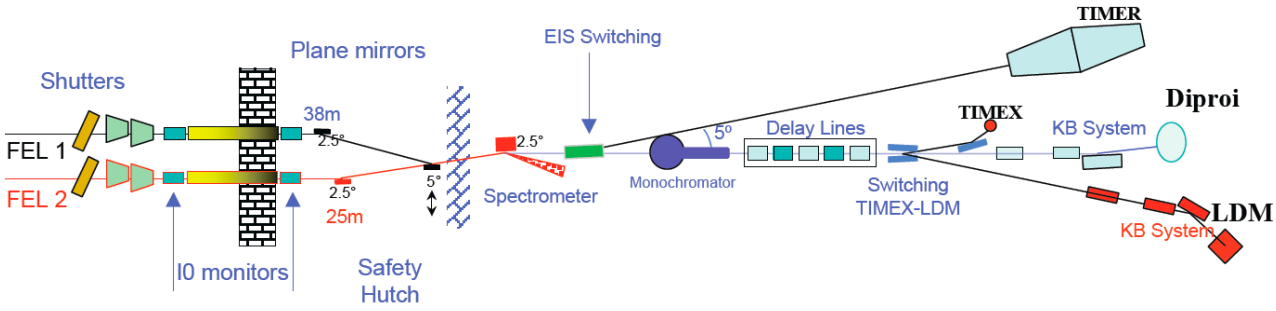
TIMER
Plane mirrors
EIS Switching
Shutters
Diproi
38m
2.5°
TIMEX
Delay Lines
KB System
FEL 1
2.5°
5°
2.5°
5°
Spectrometer
Monochromator
Switching
TIMEX-LDM
FEL 2
25m
LDM
KB System
I0 monitors
Safety
Hutch